

Rapid speciation despite conservation of phenotype

Joshua S. Schiffman[†] Peter L. Ralph^{†‡}

[†]Molecular and Computational Biology, University of Southern California, Los Angeles, California 90089, U.S.A.

[‡]Departments of Mathematics and Biology & The Institute for Ecology and Evolution, University of Oregon, Eugene, Oregon 97403, U.S.A.

jsschiff@usc.edu plr@uoregon.edu

December 6, 2017

Abstract

Even if a species’ phenotype remains unchanged over evolutionary time, the underlying mechanism may have changed, as distinct molecular pathways can realize identical phenotypes. Here we use quantitative genetics and linear system theory to study how a gene network underlying a conserved phenotype evolves, as the genetic drift of small mutational changes to these molecular pathways cause a population to explore the set of mechanisms with identical phenotypes. To do this, we model an organism’s internal state as a linear system of differential equations for which the environment provides input and the phenotype is the output, in which context there exists an exact characterization of the set of all mechanisms that give the same input–output relationship. This characterization implies that selectively neutral directions in genotype space should be common and that the evolutionary exploration of these distinct but equivalent mechanisms can lead to the reproductive incompatibility of independently evolving populations. This evolutionary exploration, or *system drift*, proceeds at a rate proportional to the amount of intrapopulation genetic variation divided by the effective population size (N_e). At biologically reasonable parameter values this process can lead to substantial interpopulation incompatibility, and thus speciation, in fewer than N_e generations. This model also naturally predicts Haldane’s rule, thus providing another possible explanation of why heterogametic hybrids tend to be disrupted more often than homogametes during the early stages of speciation.

Introduction

It is an overarching goal of many biological subdisciplines to attain a general understanding of the function and evolution of the complex molecular machinery that translates an organism’s genome into the characteristics on which natural selection acts, the phenotype. For example, there is a growing body of data on the evolutionary histories and molecular characterizations of particular gene regulatory networks [Jaeger, 2011, Davidson and Erwin, 2006, Israel et al., 2016], as well as thoughtful verbal and conceptual models [True and Haag, 2001, Weiss and Fullerton, 2000, Edelman and Gally, 2001, Pavlicev and Wagner, 2012]. Mathematical models of both particular regulatory networks and the evolution of such systems in general can provide guidance where intuition fails, and thus has the potential to discover general principles in the organization of biological systems as well as provide concrete numerical predictions [Servedio et al., 2014].

The dynamics of the molecular machinery and its interactions with the environment can be mathematically described as a dynamical system [Jaeger et al., 2015]. Movement in this direction is ongoing, as researchers have begun to study the evolution of both abstract [Wagner, 1994, 1996, Siegal and Bergman, 2002, Bergman and Siegal, 2003, Draghi and Whitlock, 2015] and empirically inspired computational and mathematical models of gene regulatory networks, [e.g. Mjolsness et al., 1991, Jaeger et al., 2004, Kozlov et al., 2012, 2015, 2014, Crombach et al., 2016, Wotton et al., 2015, Chertkova et al., 2017]. It is well known that in many contexts mathematical models can fundamentally be *nonidentifiable* and/or *indistinguishable* – meaning that there can be uncertainty about an inferred model’s parameters or even its claims about causal structure, despite access to complete and perfect data [Bellman and Åström, 1970, Grewal and Glover, 1976, Walter et al., 1984]. Models with different parameter schemes, or even different mechanics can make equally

accurate predictions, but still not actually reflect the internal dynamics of the system being modelled. In control theory, where electrical circuits and mechanical systems are often the focus, it is understood that there can be an infinite number of “realizations”, or ways to reverse engineer the dynamics of a “black box”, even if all possible input and output experiments on the “black box” are performed [Kalman, 1963, Anderson et al., 1966, Zadeh and Deoser, 1976]. The fundamental nonidentifiability of chemical reaction networks is sometimes referred to as “the fundamental dogma of chemical kinetics” [Craciun and Pantea, 2008]. In computer science, this is framed as the relationship among processes that simulate one another [Van der Schaft, 2004]. Finally, the field of *inverse problems* studies those cases where, even if a one-to-one mapping between model and behavior is possible in theory, even tiny amounts of noise can make inference problems nonidentifiable in practice [Petrov and Sizikov, 2005].

Nonidentifiability is a major barrier to mechanistic understanding of real systems, but viewed from another angle, this concept can provide a starting point for thinking about externally equivalent systems – systems that evolution can explore, so long as the parameters and structures can be realized biologically. These functional symmetries manifest in convergent and parallel evolution, as well as *developmental system drift*: the observation that macroscopically identical phenotypes in even very closely related species can in fact be divergent at the molecular and sequence level [Kimura, 1981, True and Haag, 2001, Tanay et al., 2005, Tsong et al., 2006, Hare et al., 2008, Lavoie et al., 2010, Vierstra et al., 2014, Matsui et al., 2015, Dalal et al., 2016, Dalal and Johnson, 2017]. It has also been shown theoretically that substantial genetic variation for a polygenic trait can be maintained by migration between geographical regions having different genetic bases for the same, optimal trait value [?].

In this paper we outline a theoretical framework to study the evolution of biological systems, such as gene regulatory networks. We study the evolution of an optimally adapted population subject to stabilizing selection for phenotype. Even if the phenotype remains stable over evolutionary time, the underlying mechanism might not remain so, as many distinct (and mutationally connected) molecular pathways can realize identical phenotypes. Below, we first apply results from system theory which give an analytical description of the set of all linear gene network architectures that yield identical phenotypes. Since these phenotypically equivalent gene networks are not necessarily compatible with one another, system drift may result in reproductive incompatibility between populations isolated for a sufficiently long period of time, even in the absence of any sort of adaptive, selective, or environmental change. We then use quantitative genetic theory to estimate how quickly reproductive incompatibility due to system drift will manifest

It is not a new observations that there is often more than one way to do the same thing, and that this may lead to speciation. For instance, Tulchinsky et al. [2014] (and similarly ?) looked for hybrid incompatibility following regulatory sequence drift, and Porter and Johnson [2002] studied speciation in populations expressing a simple regulatory cascade. Both found rapid speciation following directional selection, but only equivocal support for speciation under models of purely neutral drift. Additionally, Fierst and Hansen [2009] observed speciation due to an increase of segregation variance under balancing selection, in models of weak to moderate, but not strong epistasis. Our model differs from previous work in that we use linear systems theory to both explore a much richer class of regulatory network models, and provide analytical expectations in large populations with complex phenotypes that would be inaccessible to population simulations.

Results

We first describe the class of models we study, motivated by gene regulatory networks. The behavior (i.e., the temporal dynamics) of such a system is determined by a collection of n coregulating molecules – such as transcription factors – as well as by external or environmental inputs. We write $\kappa(t)$ for the vector of n molecular concentrations at time t . The vector of m “inputs” determined exogenously to the system is denoted $u(t)$, and the vector of ℓ “outputs” is denoted $\phi(t)$. The output is merely a linear function of the internal state: $\phi_i(t) = \sum_j C_{ij}\kappa_j(t)$ for some matrix C . Since ϕ is what natural selection acts on, we refer to it as the *phenotype* (meaning the “visible” aspects of the organism), and in contrast refer to κ as the *kryptotype*, as it is “hidden” from direct selection. Although ϕ may depend on all entries of κ , it is usually of lower dimension than κ , and we tend to think of it as the subset of molecules relevant for survival. The

dynamics are determined by the matrix of regulatory coefficients, A , a time-varying vector of inputs $u(t)$, and a matrix B that encodes the effect of each entry of u on the elements of the kryptotype. The rate at which the i^{th} concentration changes is a weighted sum of the concentrations of the other concentrations as well as the input:

$$\begin{aligned}\dot{\kappa}(t) &= A\kappa(t) + Bu(t) \\ \phi(t) &= C\kappa(t).\end{aligned}\tag{1}$$

Furthermore, we always assume that $\kappa(0) = 0$, so that the kryptotype measures deviations from initial concentrations. Here A can be any $n \times n$ matrix, B an $n \times m$, and C any $\ell \times n$ dimensional matrix, with usually ℓ and m less than n . We think of the system as the triple (A, B, C) , which translates (time-varying) m -dimensional input $u(t)$ into the ℓ -dimensional output $\phi(t)$. Under quite general assumptions, we can write the phenotype as

$$\phi(t) = Ce^{At}\kappa(0) + \int_0^t Ce^{A(t-s)}Bu(s)ds,\tag{2}$$

which is a convolution of the input $u(t)$ with the system's *impulse response*, which we denote as $h(t) := Ce^{At}B$.

Although many different biological systems can be modeled with this approach, for clarity, we focus on gene regulatory networks. In this interpretation, A_{ij} determines how the j^{th} transcription factor regulates the i^{th} transcription factor. If $A_{ij} > 0$, then κ_j upregulates κ_i , while if $A_{ij} < 0$, then κ_j downregulates κ_i . The i^{th} row of A is therefore determined by genetic features such as the strength of j -binding sites in the promoter of gene i , factors affecting chromatin accessibility near gene i , or basal transcription machinery activity. The form of B determines how the environment influences transcription factor expression levels, and C might determine the rate of production of downstream enzymes.

Here we have assumed that the system is linear, and begins from the “zero” state ($\kappa(0) = 0$). Of course, neither of these are necessarily true for real systems, but the dynamics of most nonlinear systems can be approximated locally by a linear systems near most points. Furthermore, the ease of analyzing linear systems makes this an attractive place to start. To demonstrate this approach, we apply it to construct a simple gene network in Example 1 below.

Example 1 (An oscillator). *For illustration, we consider an extremely simplified model of oscillating gene transcription, as for instance is found in cell cycle control or the circadian rhythm. There are two genes, whose transcript concentrations are given by $\kappa_1(t)$ and $\kappa_2(t)$, and gene-2 upregulates gene-1, while gene-1 downregulates gene-2 with equal strength. Only the dynamics of gene-1 are consequential to the oscillator (perhaps the amount of gene-1 activates another downstream gene network). Lastly, both genes are equally upregulated by an exogenous signal. The dynamics of the system are described by*

$$\begin{aligned}\dot{\kappa}_1(t) &= \kappa_2(t) + u(t) \\ \dot{\kappa}_2(t) &= -\kappa_1(t) + u(t) \\ \phi(t) &= \kappa_1(t).\end{aligned}$$

In matrix form the system regulatory coefficients are given as, $A = \begin{bmatrix} 0 & 1 \\ -1 & 0 \end{bmatrix}$, $B = \begin{bmatrix} 1 \\ 1 \end{bmatrix}$, and $C = \begin{bmatrix} 1 & 0 \end{bmatrix}$. Suppose the input is an impulse at time zero (a delta function), and so its phenotype is equal to its impulse response,

$$\phi(t) = h(t) = \sin t + \cos t.$$

The system and its dynamics are referred to in Figure 1. We return to the evolution of such a system below.



Figure 1: (Left) Diagram of the gene network in Example 1, and (right) plot of the phenotype $\phi(t)$ against time t .

Equivalent gene networks

As reviewed above, some systems with identical phenotypes are known to differ, sometimes substantially, at the molecular level; systems with identical phenotypes do not necessarily have identical kryptotypes. How many different mechanisms perform the same function?

Two systems are equivalent if they produce the same phenotype given the same input, i.e., have the same input–output relationship. We say that the systems defined by (A, B, C) and $(\bar{A}, \bar{B}, \bar{C})$ are **phenotypically equivalent** if their impulse response functions are the same: $h(t) = \bar{h}(t)$ for all $t \geq 0$. This implies that for any acceptable input $u(t)$, if $(\kappa_u(t), \phi_u(t))$ and $(\bar{\kappa}_u(t), \bar{\phi}_u(t))$ are the solutions to equation (1) of these two systems, respectively, then

$$\phi_u(t) = \bar{\phi}_u(t) \quad \text{for all } t \geq 0.$$

In other words, phenotypically equivalent systems respond identically for *any* input.

One way to find other systems phenotypically equivalent to a given one is by change of coordinates: if V is an invertible matrix, then the systems (A, B, C) and (VAV^{-1}, VB, CV^{-1}) are phenotypically equivalent because their impulse response functions are equal:

$$\begin{aligned} h(t) &= Ce^{At}B = CV^{-1}Ve^{At}V^{-1}VB \\ &= CV^{-1}e^{VAV^{-1}t}VB = \bar{C}e^{\bar{A}t}\bar{B} = \bar{h}(t). \end{aligned} \tag{3}$$

However, not all phenotypically equivalent systems are of this form: systems can have identical impulse responses without being coordinate changes of each other. In fact, systems with identical impulse responses can involve interactions between different numbers of molecules, and thus have kryptotypes in different dimensions altogether.

This implies that most systems have at least n^2 degrees of freedom, where recall n is the number of components of the kryptotype vector. This is because for an arbitrary $n \times n$ matrix Z , taking V to be the identity matrix plus a small perturbation in the direction of Z above implies that moving A in the direction of $ZA - AZ$ while also moving B in the direction of ZB and C in the direction of $-CZ$ will leave the phenotype unchanged to second order in the size of the perturbation. If the columns of B and the rows of C are not all eigenvectors of A , then any such Z will result in a different system.

It turns out that in general, there are more degrees of freedom, except if the system is *minimal* – meaning, informally, that it uses the smallest possible number of components to achieve the desired dynamics. Results in system theory show that any system can be realized in a particular minimal dimension (the dimension of the kryptotype, n_{\min}), and that any two phenotypically equivalent systems of dimension n_{\min} are related by a change of coordinates. Since gene networks can grow or shrink following gene duplications and deletions, these additional degrees of freedom can apply in principle to any system.

Even if the system is not minimal, results from systems theory explicitly describe the set of all phenotypically equivalent systems. We refer to $\mathcal{N}(A_0, B_0, C_0)$ as the set of all systems phenotypically equivalent to the system defined by (A_0, B_0, C_0) :

$$\mathcal{N}(A_0, B_0, C_0) = \{(A, B, C) : Ce^{At}B = C_0e^{A_0t}B_0 \text{ for } t \geq 0\}. \quad (4)$$

These systems need not have the same kryptotypic dimension n , but must have the same input and output dimensions (ℓ and m , respectively).

The Kalman decomposition, which we now describe informally, elegantly characterizes this set [Kalman, 1963, Kalman et al., 1969, Anderson et al., 1966]. To motivate this, first note that the input $u(t)$ only directly pushes the system in certain directions (those lying in the span of the columns of B). As a result, different combinations of input can move the system in any direction that lies in what is known as the *reachable subspace*. Analogously, we can only observe motion of the system in certain directions (those lying in the span of the rows of C), and so can only infer motion in what is known as the *observable subspace*. The Kalman decomposition then classifies each direction in kryptotype space as either reachable or unreachable, and as either observable or unobservable. Only the components that are both reachable and observable determine the system's phenotype – that is, components that both respond to an input and produce an observable output.

Concretely, the **Kalman decomposition** of a system (A, B, C) gives a change of basis P such that the transformed system (PAP^{-1}, PB, CP^{-1}) has the following form:

$$PAP^{-1} = \begin{bmatrix} A_{r\bar{o}} & A_{r\bar{o},ro} & A_{r\bar{o},\bar{r}\bar{o}} & A_{r\bar{o},\bar{r}o} \\ 0 & A_{ro} & 0 & A_{ro,\bar{r}o} \\ 0 & 0 & A_{\bar{r}\bar{o}} & A_{\bar{r}\bar{o},\bar{r}o} \\ 0 & 0 & 0 & A_{\bar{r}o} \end{bmatrix},$$

and

$$PB = \begin{bmatrix} B_{r\bar{o}} \\ B_{ro} \\ 0 \\ 0 \end{bmatrix} \quad (CP^{-1})^T = \begin{bmatrix} 0 \\ C_{ro}^T \\ 0 \\ C_{\bar{r}o}^T \end{bmatrix}.$$

The impulse response of the system is given by

$$h(t) = C_{ro}e^{A_{ro}t}B_{ro},$$

and therefore, the system is phenotypically equivalent to the *minimal* system (A_{ro}, B_{ro}, C_{ro}) .

This decomposition is unique up to a change of basis that preserves the block structure. In particular, the minimal subsystem obtained by the Kalman decomposition is unique up to a change of coordinates. This implies that there is no equivalent system with a smaller number of kryptotypic dimensions than the dimension of the minimal system. It is remarkable that the gene regulatory network architecture to achieve a given input–output map is never unique – both the change of basis used to obtain the decomposition and, once in this form, all submatrices other than A_{ro} , B_{ro} , and C_{ro} can be changed without affecting the phenotype, and so represent degrees of freedom. (However, some of these subspaces may affect how the system deals with noise.)

Note on implementation: The *reachable subspace*, which we denote by \mathcal{R} , is defined to be the closure of $\text{span}(B)$ under applying A , and the *unobservable subspace*, denoted $\bar{\mathcal{O}}$, is the largest A -invariant subspace contained in the null space of C . The four subspaces, $r\bar{o}$, ro , $\bar{r}\bar{o}$, and $\bar{r}o$ are defined from these by intersections and orthogonal complements – ro refers to the both *reachable and observable* subspace, while $\bar{r}\bar{o}$ refers to the *unreachable and unobservable* subspace, and similarly for $\bar{r}o$ and $r\bar{o}$.

For the remainder of the paper, we interpret \mathcal{N} as the neutral set in the fitness landscape, along which a large population will drift under environmental and selective stasis. Even if the phenotype is constrained and

remains constant through evolutionary time, the molecular mechanism underpinning it is not constrained and likely will not be conserved.

Finally, note that if B and C are held constant – i.e., if the relationships between environment, kryptotype, and phenotype do not change – there are *still* usually degrees of freedom. The following example 2 gives the set of minimal systems equivalent to the oscillator of Example 1, that all share common B and C matrices. The oscillator can also be equivalently realized by a three-gene (or larger) network, and will have even more evolutionary degrees of freedom available, as in Figure 3.

Example 2 (All phenotypically equivalent oscillators). *The oscillator of example 1 is minimal, and so any equivalent system is a change of coordinates by an invertible matrix V . If we further require B and C to be invariant then we need $VB = B$ and $CV = C$. Therefore the following one-parameter family $(A(\tau), B, C)$ describes the set of all two-gene systems phenotypically equivalent to the oscillator:*

$$A(\tau) = \frac{-1}{\tau + 1} \begin{bmatrix} -\tau & -1 \\ 2\tau(\tau + 1) + 1 & \tau \end{bmatrix} \text{ for } \tau \neq -1.$$

The resulting set of systems are depicted in Figure 2.

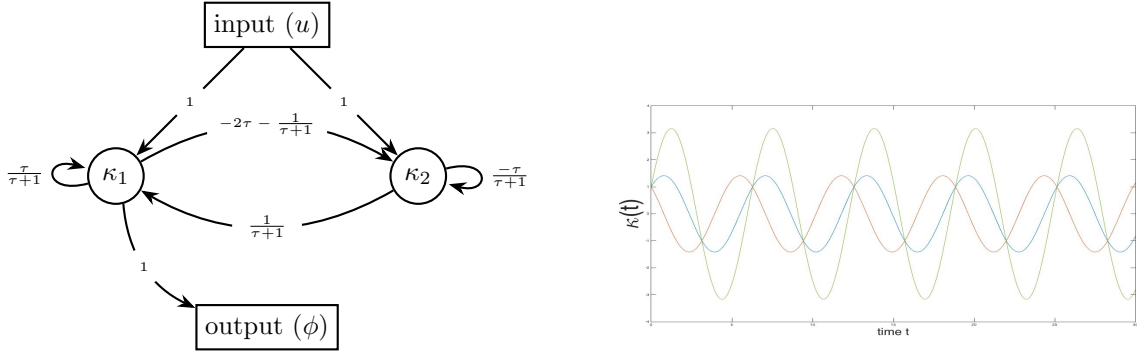


Figure 2: (Left) $A(\tau)$, the set of all phenotype-equivalent cell cycle control networks. (Right) Gene-1 dynamics (blue) for both systems $A(0)$ and $A(-2)$ are identical, however, $A(0)$ gene-2 dynamics (orange) differ from $A(-2)$ (green).

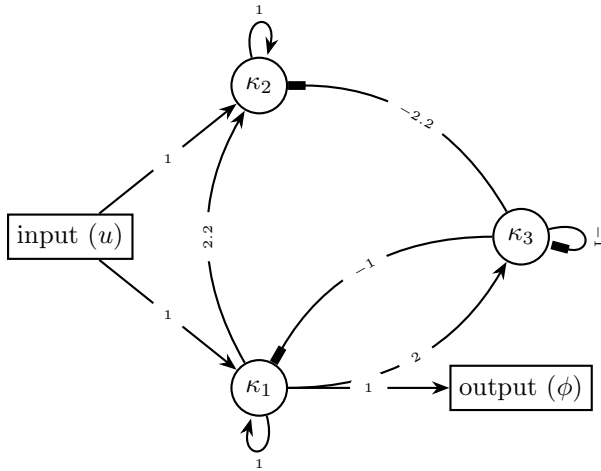


Figure 3: A possible non-minimal three-gene oscillator, phenotypically equivalent to $A(\tau)$, the systems in Examples 1 and 2.

Sexual reproduction and recombination Parents with phenotypically equivalent yet differently wired gene networks may produce offspring with dramatically different phenotypes. If the phenotypes are significantly divergent then the offspring may be inviable or otherwise dysfunctional, despite both parents being well adapted. If this is consistent for the entire population, we would consider them to be separate species, in accord with the biological species concept [Mayr, 2000].

First, we must specify how sexual reproduction acts on these systems. Suppose that each of a diploid organisms' two genomes encodes a set of system coefficients. We assume that a diploid which has inherited systems (A', B', C') and (A'', B'', C'') from its two parents has phenotype determined by the system that averages these two, $((A' + A'')/2, (B' + B'')/2, (C' + C'')/2)$.

Each genome an organism inherits is generated by meiosis, in which both of its diploid parents recombine their two genomes, and so an F_1 offspring carries one system copy from each parent, and an F_2 is an offspring of two independently formed F_1 s. If the parents are from distinct populations, these are simply first- and second-generation hybrids, respectively.

Exactly how the coefficients (i.e., entries of A , B or C) of a haploid system inherited by an offspring from her diploid parent are determined by the parent's two systems depends on the genetic basis of any variation in the coefficients. Thanks to the randomness of meiotic segregation, the result is random to the extent that each parent is heterozygous for alleles that affect the coefficients. Since the i^{th} row of A summarizes how each gene regulates gene i , and hence is determined by the promoter region of gene i , the elements of a row of A tend to be inherited together, which will create covariance between entries of the same row. It is, however, a quite general observation that the variation seen among recombinant systems is proportional to the difference between the two parental systems. This is certainly true if each coefficient is determined by a single nonrecombining locus, so that each coefficient in the system produced by meiosis is an independent random choice between the two parental coefficients. On the other hand, if a coefficient is determined by additive contributions of independently segregating loci, then the law of total variance applied after conditioning on the parental origin of each allele implies that the variance is equal to one-quarter of the squared difference between parental coefficients.

Offspring formed from two phenotypically identical systems do not necessarily exhibit the same phenotype as both of its parents – in other words \mathcal{N} , the set of all systems phenotypically equivalent to a given one, is not, in general, closed under averaging or recombination. If sexual recombination among systems drawn from \mathcal{N} yields systems with divergent phenotypes, populations containing significant diversity in \mathcal{N} can carry genetic load, and isolated populations may fail to produce hybrids with viable phenotypes.

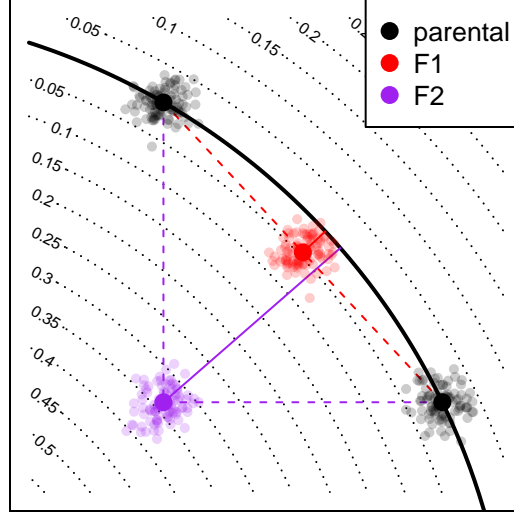


Figure 4: A conceptual figure of the fitness consequences of hybridization: axes represent system coefficients (i.e., entries of A); the line of optimal system coefficients is down in black; dotted lines give phenotypic distances to the optimum. A pair of parental populations are shown in black, along the optimum; a hypothetical population of F_1 s are shown in red, and the distribution of one type of F_2 is shown in purple (other types of F_2 are not shown; some would be a similar distance to the other side of the optimal set). The distribution of F_2 s is appropriate for mixed homozygotes if both traits have a simple, one-locus genetic basis, but there is variation within each population at that locus.

Hybrid incompatibility

Two parents with the optimal phenotype can produce offspring whose phenotype is suboptimal if the parents have different underlying systems. How quickly do hybrid phenotypes break down as genetic distance between parents increases? We will quantify how far a system’s phenotype is from optimal using a weighted difference between impulse response functions. Suppose that $\rho(t)$ is a nonnegative, smooth, square-integrable weighting function, $h_0(t)$ is the *optimal* impulse response function and define the “distance to optimum” of another impulse response function to be

$$D(h) = \left(\int_0^\infty \rho(t) \|h(t) - h_0(t)\|^2 dt \right)^{1/2}. \quad (5)$$

Consider reproduction between a parent with system (A, B, C) and another displaced by distance ϵ in the direction (X, Y, Z) , i.e., having system $(A + \epsilon X, B + \epsilon Y, C + \epsilon Z)$. We assume both are “perfectly adapted” systems, i.e., having impulse response function $h_0(t)$, and their offspring has impulse response function $h_\epsilon(t)$. A Taylor expansion of $D(h_\epsilon)$ in ϵ is explicitly worked out in Appendix A.2, and shows that the phenotype of an F_1 hybrid between these two is at distance proportional to ϵ^2 from optimal, while F_2 hybrids are at distance proportional to ϵ . This is because an F_1 hybrid has one copy of each parental system, and therefore lies directly between the parental systems (see Figure 4) – the parents both lie in \mathcal{N} , which is the valley defined by D , and so their midpoint only differs from optimal due to curvature of \mathcal{N} . In contrast, an F_2 hybrid may be homozygous for one parental type in some coefficients and homozygous for the other parental type in others; this means that each coefficient of an F_2 may be equal to either one of the parents, or intermediate between the two; this means that possible F_2 systems may be as far from the optimal set, \mathcal{N} , as the distance between the parents. The precise rate at which the phenotype of a hybrid diverges depends on the geometry of the optimal set \mathcal{N} relative to segregating genetic variation.

Example 3 (Hybrid Incompatibility in the Oscillator). *Offspring of two equivalent systems from Example 2 can easily fail to oscillate. For instance, the F_1 offspring between homozygous parents at $\tau = 0$ and $\tau = -2$ has phenotype $\phi_{F_1}(t) = e^t$, rather than $\phi(t) = \sin t + \cos t$. However, the coefficients of these two parental systems differ substantially, probably more than would be observed between diverging populations. In figure 5 we compare the phenotypes for F_1 and F_2 hybrids between more similar parents, and see increasingly divergent phenotypes as the difference between the parental systems increases. (In this example, the coefficients of $A(\epsilon)$ differ from those of $A(0)$ by an average factor of $1 + \epsilon/2$; such small differences could plausibly be caused by changes to promoter sequences.) This divergence is quantified in Figure 6, which shows that mean distance to optimum phenotype of the F_1 and F_2 hybrid offspring between $A(0)$ and $A(\epsilon)$ increases with ϵ^2 and ϵ , respectively.*



Figure 5: **(left)** Phenotypes of F_1 hybrids between an $A(0)$ parent and, top-to-bottom, an $A(1/100)$, an $A(1/10)$, and $A(1/2)$ parent; parental coefficients differ by around 0.5%, 5%, and 25% respectively. Parental phenotypes ($\sin t + \cos t$) are shown in solid black, and hybrid phenotypes in dashed blue. **(right)** Phenotypes of all possible F_2 hybrids between the same set of parents, with parental phenotype again in black. Different colored lines correspond to different F_2 s; note that some completely fail to oscillate.



Figure 6: Phenotype distance to optimum, D , using $\rho(t) = \exp(-t/4\pi)$ for F_1 (black) and F_2 (blue) hybrids between an $A(0)$ and an $A(\epsilon)$ parent. Genetic distance is computed as $\sqrt{\sum_{ij}(A_{ij}(0) - A_{ij}(\epsilon))^2}$.

Haldane’s rule This model naturally predicts Haldane’s rule, the observation that if only one hybrid sex is sterile or inviable it is likely the heterogametic sex (e.g., the male in XY sex determination systems) [Haldane, 1922]. For example, consider an XY species with a two-gene network where the first gene resides on an autosome and the second gene on the X chromosome. A male whose pair of haplotypes is $(\begin{bmatrix} A_1 & A_2 \\ X_1 & X_2 \end{bmatrix}, \begin{bmatrix} A_1 & A_2 \\ X_1 & X_2 \end{bmatrix})$ has phenotype determined by $A = \begin{bmatrix} A_1 & A_2 \\ X_1 & X_2 \end{bmatrix}$, if dosage compensation upregulates heterogametes by a factor of 2 relative to homogametes, while a female homozygous for the haplotype $\begin{bmatrix} \bar{A}_1 & \bar{A}_2 \\ \bar{X}_1 & \bar{X}_2 \end{bmatrix}$, has phenotype determined by $A = \begin{bmatrix} \bar{A}_1 & \bar{A}_2 \\ \bar{X}_1 & \bar{X}_2 \end{bmatrix}$. An F_1 male offspring of these two will have its phenotype determined by $\begin{bmatrix} (A_1 + \bar{A}_1)/2 & (A_2 + \bar{A}_2)/2 \\ \bar{X}_1 & \bar{X}_2 \end{bmatrix}$. If both genes resided on the autosomes this system would only be possible in an F_2 cross. More generally, if the regulatory coefficients for a system are shared between the sex and one or more autosomal chromosomes, F_1 males are effectively equivalent to purely autosomal-system F_2 s. In this setting, Haldane’s rule is mechanistically similar to *hybrid breakdown*, the observation that F_2 s will often be less fit than F_1 hybrid crosses, in the early stages of speciation. This mechanism relies on the genetic variation of a system being shared across the sex chromosomes and the autosomes, and appears to be distinct from the “dominance”, “faster-X”, and “faster-male” theories [Orr, 1997, Coyne and Orr, 1998, Turelli and Orr, 1995] usually suggested to explain Haldane’s rule.

System drift and the accumulation of incompatibilities

Thus far we have seen that many distinct molecular mechanisms can realize identical phenotypes and that these mechanisms may fail to produce viable hybrids. This begs the question: does evolution shift molecular mechanisms fast enough to be a significant driver of speciation? To approach this question, we explore a general quantitative genetic model in which a population drifts stochastically near a set of equivalent and optimal systems due to the action of recombination, mutation, and demographic noise. Although this is motivated by the results on linear systems above, the quantitative genetics calculations are more general,

and only depend on the presence of genetic variation and a continuous set of phenotypically equivalent systems.

We will suppose that each organism’s phenotype is determined by its vector of coefficients, denoted by $x = (x_1, x_2, \dots, x_p)$, and that the corresponding fitness is determined by the distance of its phenotype to optimum. The optimum phenotype is unique, but is realized by many distinct x – those falling in the “optimal set” \mathcal{N} . The phenotypic distance to optimum of an organism with coefficients x is denoted $D(x)$. In the results above, $x = (A, B, C)$ and $D(x)$ is given by equation (5). The fitness of an organism with coefficients x will be $\exp(-D(x)^2)$. We assume that in the region of interest, the map D is smooth and that we can locally approximate the optimal set \mathcal{N} as a quadratic surface. As above, an individual’s coefficients are given by averaging its parentally inherited coefficients and adding random noise due to segregation and possibly new mutation. Concretely, we use the *infinitesimal model* for reproduction [Barton et al., 2016] – the offspring of parents at x and x' will have coefficients $(x + x')/2 + \varepsilon$, where ε is a random Gaussian displacement due to random assortment of parental alleles.

System drift We work with a randomly mating population of effective size N_e . If the population variation has standard deviation σ in a particular direction, since subsequent generations resample from this diversity, the population mean coefficient will move a random distance of size $\sigma/\sqrt{N_e}$ per generation, simply because this is the standard deviation of the mean of a random sample [Lande, 1981]. Selection will tend to restrain this motion, but movement along the optimal set \mathcal{N} is unconstrained, and so we expect the population mean to drift along the optimal set like a particle diffusing. The amount of variance in particular directions in coefficient space depends on constraints imposed by selection and correlations between the genetic variation underlying different coefficients (the G matrix [Arnold et al., 2008]). It therefore seems reasonable to coarsely model the time evolution of population variation in regulatory coefficients as a “cloud” of width σ about the population mean, which moves as an unbiased Brownian motion through the set of network coefficients that give the optimal phenotype.

Next, we calculate with some simplifying assumptions to give the general idea; multivariate derivations appear in Appendix B. There will in general be different amounts of variation in different directions; to keep the discussion intuitive, we only discuss σ_N , the amount of variation in “neutral” directions (i.e., directions along \mathcal{N}), and σ_S , the amount of variation in “selected” directions (perpendicular to \mathcal{N}). The other relevant scale we denote by γ , which is the scale on which distance to phenotypic optimum changes as x moves away from the optimal set, \mathcal{N} . Concretely, γ is $1/(\frac{d}{du}D(x+uz))$ where x is optimal and z is a “selected” direction perpendicular to \mathcal{N} . With these parameters, a typical individual will have a fitness of around $\exp(-(\sigma_S/\gamma)^2)$. Of course, there are in general many possible neutral and selected directions; we take γ to be an appropriate average over possible directions.

Hybridization The means of two allopatric populations each of effective size N_e separated for T generations will be a distance roughly of order $2\sigma_N\sqrt{T/N_e}$ apart along \mathcal{X} . (Consult figure 4 for a conceptual diagram.) A population of F_1 hybrids has one haploid genome from each, whose coefficients are averaged, and so will have mean system coefficients at the midpoint between their means. The distribution of F_2 s will have mean at the average of the two populations, but will have higher variance. The variance of F_2 s can be shown to increase linearly with the square of the distance between parental population means under models of both simple and polygenic traits. This is suggested by figure 4 and shown in Appendix B.1. Concretely, we expect the population of F_1 s to have variance σ_S^2 in the selected direction (the same as within each parental population), but the population of F_2 s will have variance of order $\sigma_S^2 + 4\omega\sigma_N^2T/N_e$, where ω is a factor that depends on the genetic basis of the coefficients. If the optimal set \mathcal{N} has dimension q , using the polygenic model of appendix B.1, ω is proportional to the number of degrees of freedom: $\omega = (p - q)/8$. If each trait is controlled by a single locus, as in figure 4, the value is similar.

What are the fitness consequences? A population of F_2 s will begin to be substantially less fit than the parents once they differ from the optimum by a distance of order γ , i.e., once $\sqrt{4\omega T/N_e} \approx \gamma/\sigma_N$. This implies that hybrid incompatibility among F_2 s should appear much slower – on a time scale of $N_e(\gamma/\sigma_N)^2/(4\omega)$ generations. The F_1 s will not suffer fitness consequences until the hybrid mean is further than γ from the

optimum; as shown in appendix A.1 (and suggested by figure 4), this deviation of the mean from optimum grows with the square of the distance between the parental populations, and so we expect fitness costs in F_1 s to appear on a time scale of N_e^2 generations.

For a more concrete prediction, suppose that the distribution among hybrids is Gaussian. A population whose trait distribution is Gaussian with mean μ and variance σ , has mean fitness

$$\int_{-\infty}^{\infty} \frac{1}{\sigma\sqrt{2\pi}} e^{-\frac{(x-\mu)^2}{2\sigma^2}} e^{-\frac{x^2}{2\gamma^2}} dx = \sqrt{\frac{1}{1+\sigma^2/\gamma^2}} \exp\left\{-\frac{\mu^2}{\gamma^2} \left(\frac{1}{1+\sigma^2/\gamma^2}\right)\right\}. \quad (6)$$

This assumes a single trait, for simplicity. A population of F_2 s will have, as above, variance $\sigma^2 = \sigma_S^2 + 4\omega\sigma_N^2 T/N_e$. The mean diverges with the square of the distance between the parentals, so we set $\mu = c_\mu \gamma T/N_e$, where c_μ is a constant depending on the local geometry of the optimal set. The mean fitness in parental populations is as in equation 6 with $\mu = 0$ and $\sigma = \sigma_S$. This implies that if we define $\mathcal{F}_2(T)$ to be the mean relative fitness among F_2 hybrids between two populations separated by T generations, (i.e., the mean fitness divided by the mean fitness of the parents) then

$$\mathcal{F}_2(T) = \left(1 + \frac{4\omega(\sigma_N/\gamma)^2}{(1 + (\sigma_S/\gamma)^2)} \frac{T}{N_e}\right)^{-1/2} \exp\left\{-\left(c_\mu \frac{T}{N_e}\right)^2 \left(\frac{1}{1 + (\sigma_S/\gamma)^2 + 4\omega(\sigma_N/\gamma)^2 T/N_e}\right)\right\}. \quad (7)$$

If each of the q selected directions acts independently, the drop in fitness will be $\mathcal{F}_2(T)^q$; the expression for the correlated, multivariate case is given in Appendix B.1. We discuss the implications of this expression in the next section.

Speciation rates under neutrality Equation (7) describes how fast hybrids become inviable as the time that the parental populations are isolated increases; what does this tell us about speciation rates under neutrality? From equation (7) we observe that time is always scaled in units of N_e generations, the population standard deviations are always scaled by γ , and the most important term is the rate of accumulation of segregation variance, $4\omega(\sigma_N/\gamma)^2$. All else being equal, this process will lead to speciation more quickly in smaller populations and in populations with more neutral genetic variation (larger σ_N). These parameters are related – larger populations generally have more genetic variation – but since these details depend on the situation, we leave these separate.

How does this prediction depend on the system size and constraint? If there are p trait dimensions, constrained in q dimensions, and if ω is proportional to $p - q$, then the rate that F_2 fitness drops is, roughly, $(1 + 4(p - q)KT/N_e)^{-q/2} \propto q(p - q)$, where K is a constant. Both degree of constraint and number of available neutral directions affect the speed of accumulation of incompatibilities – more unconstrained directions allows faster system drift, but more constrained directions implies greater fitness consequences of hybridization. However, note that in real systems, it is likely that γ also depends on p and q .

Now we will interpret equation (7) in three situations plausible for different species, depicting how hybrid fitness drops as a function of T/N_e in Figure 7. In all cases, the fitness drop for F_1 hybrids is much smaller than that of F_2 s, so we work only with the first (square-root) term in equation (7).

Suppose in a large, genetically diverse population, the amount of heritable variation in the neutral and selected directions are roughly equal ($\sigma_N \approx \sigma_S$) but the overall amount of variation is (weakly) constrained by selection ($\sigma_N \approx \gamma$). If so, then the first term of equation (7) is $1/\sqrt{1 + 2\omega T/N_e} \approx 1 - \omega T/N_e$. If also $\omega = 1$, then, for instance, after $0.1N_e$ generations the average F_2 fitness has dropped by 10% relative to the parentals.

Consider instead a much smaller, isolated population whose genetic variation is primarily constrained by genetic drift, so that $\sigma_N \approx \sigma_S \ll \gamma$. Setting $a = (\sigma_N/\gamma)^2$ to be small, the fitness of F_2 s is $\mathcal{F}_2 \leq 1/\sqrt{1 + 4\omega a T/N_e} \approx 1 - 2\omega a T/N_e$. Hybrid fitness seems to drop more slowly in this case in figure 7, but since time is scaled by N_e , so speciation may occur *faster* than in a large population. However, at least in some models [?], in small populations at mutation-drift equilibrium the amount of genetic variance (σ_N^2) is proportional to N_e , which would compensate for this difference, perhaps even predicting the rate of decrease of hybrid fitness to be *independent* of population size for small populations.

In the other direction, consider large metapopulations (or a “species complex”) among which heritable variation is strongly constrained by selection (i.e., there is substantial recombination load), so that $\sigma_S \approx \gamma$ but σ_N/γ is large. Then the fitness of F_2 s is $\mathcal{F}_2 \leq 1/\sqrt{1 + 2\omega aT/N_e} \approx 1 - \omega aT/N_e$, and could be extremely rapid if a is large.

For instance, between two populations of one million organisms that has 10 generations per year (a drosophilid species, perhaps) under the “large population” scenario of Figure 7A, system drift would lead to a substantial fitness drop of around 10% in F_2 hybrids in only 10,000 years. This drop may be enough to induce evolutionary reinforcement of reproductive isolation. If one thousand of these organisms is isolated (perhaps on an island, as in Figure 7B), then a similar drop could occur in around 120 years. On the other hand, if the population is one of several of similar size that have recently come into secondary contact after population re-expansion, the situation may be similar to that of Figure 7C with $N_e = 10^6$, and so the same drop could occur after 1,100 years. (However, hyperdiverse populations of this last type may not be stable on these time scales.)

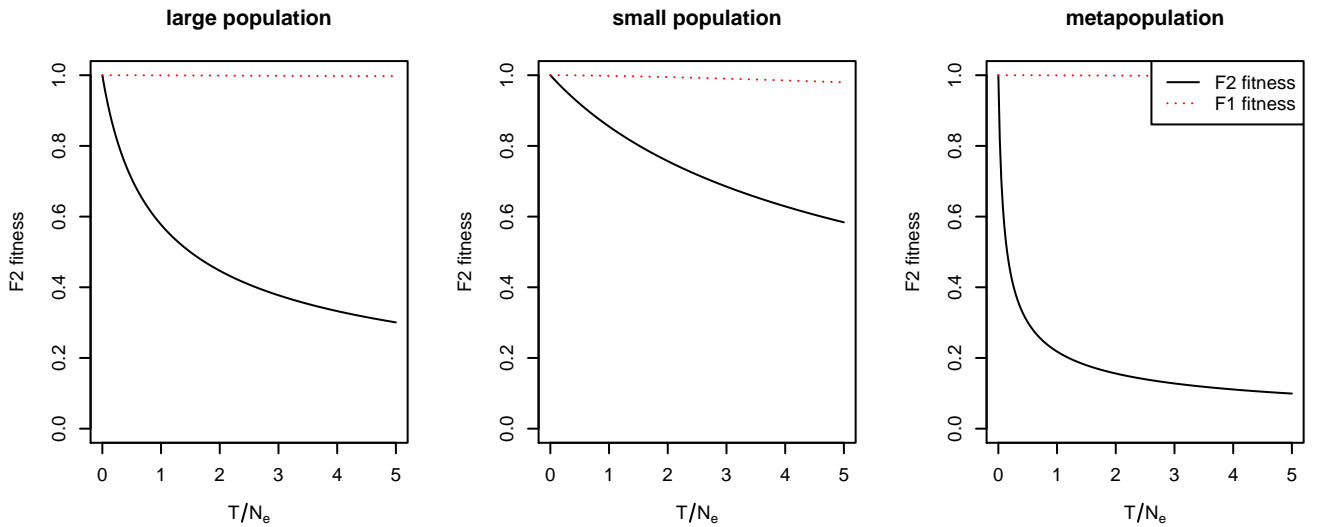


Figure 7: Mean drop of F_1 and F_2 fitness relative to parental species, with $\omega = 1$ and (A) $\sigma_N^2 = \sigma_S^2 = \gamma^2$ (B) $\sigma_N^2 = \sigma_S^2 = 0.1\gamma^2$ (C) $0.1\sigma_N^2 = \sigma_S^2 = \gamma^2$. The F_2 fitness is from equation (7), and the F_1 fitness is determined only by the exponential term of that equation. is small relative to that of increased variance.

Genetic variation in empirical regulatory systems

What is known about the key quantity above, the amount of heritable variation in real regulatory networks? The coefficient A_{ij} from the system (1) measures how much the rate of net production of i changes per change in concentration of j . It is generally thought that regulatory sequence change contributes much more to inter- and intraspecific variation than does coding sequence change affecting molecular structure [?]. In the context of transcription factor networks this may be affected not only by the binding strength of molecule j to the promoter region of gene i but also the effects of other transcription factors (e.g., cooperativity) and local chromatin accessibility [Stefflova et al., 2013]. For this reason, the mutational target size for variation in A_{ij} may be much larger than the dozens of base pairs typically implicated in the handful of binding sites for transcription factor j of a typical promoter region, and single variants may affect many entries of \mathcal{N} simultaneously.

Variation in binding site occupancy may overestimate variation in A , since it does not capture buffering effects (if for instance only one site of many needs to be occupied for transcription to begin), and variation

in expression level measures changes in steady-state concentration (our κ_i) rather than the *rate* of change. Nonetheless, these measures likely give us an idea of the scale of variability. [Kasowski et al. \[2010\]](#) found differential occupancy in 7.5% of binding sites of a transcription factor (p65) between human individuals. [Verlaan et al. \[2009\]](#) showed that cis-regulatory variation accounts for around 2–6% of expression variation in human blood-derived primary cells, while [Lappalainen et al. \[2013\]](#) found that human population variation explained about 3% of expression variation. Studying natural flycatcher populations, [? \[2013\]](#) found that 7.2–8.5% of transcripts showed allele-specific expression – indicative of standing genetic *cis*-regulatory variation. Similarly, in wild baboons, [? \[2013\]](#) observed allele-specific expression in 23.4% of genes studied. Taken together, this suggests that variation in the entries of A may be on the order of at least a few percent between individuals of a population – doubtless varying substantially between species and between genes.

Discussion

Above we synthesize concepts and tools from molecular and evolutionary biology with tools from control theory to study the evolution of a mechanistic model of the molecular genotype-phenotype map under stabilizing selection. This model allows us to analytically describe the processes discussed verbally as phenogenetic drift [[Weiss and Fullerton, 2000](#)] and developmental system drift [[True and Haag, 2001](#)]. In this context, the Kalman decomposition [[Kalman, 1963](#)] gives an analytical description of all phenotypically equivalent gene networks. It also implies that nearly all systems are nonidentifiable, and hence the general existence of axes of genetic variation that are not constrained by selection. The independent movement of separated populations along these axes can lead to reduction in hybrid viability, and hence speciation, at a speed that depends on effective population size and amount of genetic variation. In this model, at biologically reasonable parameter values, system drift is a significant – and possibly rapid – driver of speciation. This may at first be surprising because hybrid inviability appears as a consequence of recombining different, yet functionally equivalent, mechanisms.

Consistent with empirical observation of hybrid breakdown [e.g. [Plötner et al., 2017](#)], we see that the fitnesses of F_2 hybrids drop at a much faster rate than those of F_1 s. Another natural consequence of the model is Haldane’s rule, that if only one F_1 hybrid sex is inviable or sterile it is likely to be the heterogametic sex. This occurs because if the genes underlying a regulatory network are distributed among both autosomes and the sex chromosome, then heterogametic F_1 s show variation similar to that seen in F_2 s.

Is there evidence that this is actually occurring? System drift and network rewiring has been inferred across the tree of life [[Wotton et al., 2015](#), [Crombach et al., 2016](#), [Dalal and Johnson, 2017](#), [Johnson, 2017](#), [?](#)], and there is often significant regulatory variation segregating within populations. Transcription in hybrids between closely related species with conserved transcriptional patterns can also be divergent [[Haerty and Singh, 2006](#), [Maheshwari and Barbash, 2012](#), [Coolon et al., 2014](#), [Michalak and Noor, 2004](#), [Mack and Nachman, 2016](#)], and hybrid incompatibilities have been attributed to cryptic molecular divergence underlying conserved body plans [[Gavin-Smyth and Matute, 2013](#)]. Furthermore, in cryptic species complexes (e.g., sun skinks [[Barley et al., 2013](#)]), genetically distinct species may be nearly morphologically indistinguishable.

The origin of species not by means of natural selection? Although, as classically formulated, the Dobzhansky-Muller model of hybrid incompatibility is agnostic to the relative importance of neutral versus selective genetic substitutions [[Coyne and Orr, 1998](#)], and plausible mechanisms for the origin of Dobzhansky–Muller incompatibilities by neutral genetic drift have been proposed [[Lynch and Force, 2000](#)] and under stabilizing selection [[Fierst and Hansen, 2009](#)], previous authors have argued that neutral processes are likely too slow to be a significant driver of speciation [[Nei et al., 1983](#), [Seehausen et al., 2014](#)]. (Also note that the mechanism underlying hybrid inviability here resembles the Dobzhansky-Muller model, but is more similar to the “pathway model” of [Lindtke and Buerkle \[2015\]](#).) Using simulations, [Porter and Johnson \[2002\]](#) demonstrated the accumulation of hybrid incompatibilities under directional, but not stabilizing selection, and [Palmer and Feldman \[2009\]](#) observed the appearance of incompatibilities in populations evolving in a constant environment, only if the populations were suboptimally adapted. This, in light of the few known incompatibilities, has lead some to conclude that hybrid incompatibility is typically a byproduct of positive

selection [Orr et al., 2004, Schluter, 2009] or a consequence of genetic conflict [Presgraves, 2010, Crespi and Nosil, 2013]. In contrast, the model we develop here suggests that even under strictly neutral conditions, system drift can lead to speciation, at a rate fast enough to play a substantial role in species formation across the tree of life. Our results show that hybrids, under neutral processes, break down as a function of genetic distance, and so may, in part, explain broad patterns such as the relationship between molecular divergence and genetic isolation seen by Roux et al. [2016], and the clocklike speciation patterns observed by Hedges et al. [2015].

All of these forces – adaptive shifts, conflict, and network drift – are plausible drivers of speciation, and may even interact. For instance, reinforcement due to local adaptation could in some situations provide a selective pressure that speeds up system drift. It remains to be seen how the relative strengths of these forces compare. Furthermore, while the fitness consequences of incompatibility in any one given network may be small, the cumulative impact of system drift across the many different networks an organism relies on may be substantial.

Of course the basic assumptions of this model will be violated in practice (constant selective pressures, etc.), however, this model can function as a “neutral null” description of gene network evolution (a strategy advocated for by Lynch [2007], Fay and Wittkopp [2008], Koonin [2016]). If this model succeeds in describing actual system evolution, it can be inferred that the mechanism underlying species formation does not require the inclusion of adaptation or changes in selection to explain the emergence of hybrid incompatibility.

Population isolates and genetic load Above we have mostly discussed the case of two separated populations of equal size. In contrast, consider a small subset of a large population that is suddenly isolated. It will have a large amount of genetic variance, thanks to its history, but a small population size – and so can drift quite quickly until it exhausts its genetic variation. By this point, it could have accumulated substantial incompatibility with the parental population. Similarly, in a species with substantial isolation by distance, geographically local systems drift might lead to genetic load due only to recombination, much as in [?].

Nonlinearity and model assumptions Of course, real regulatory networks are not linear dynamical systems. Most notably, physiological limits put upper bounds on expression levels, implying saturating response curves. It remains to be seen how well these results carry over into real systems, but the fact that most nonlinear systems can be locally approximated by a linear one suggests our qualitative results may hold more generally. Furthermore, nonidentifiability (which implies the existence of neutral directions) is often found in practice in moderately complex models of biological systems [Gutenkunst et al., 2007, Piazza et al., 2008].

This simple quantitative genetics model we use above has been shown to produce good predictions in many situations, even when the substantial number of simplifying assumptions are violated [Turelli and Barton, 1994]. The calculations above should be fairly robust even to substantial deviations from normality. A larger effect on these predictions seems likely due to correlations due to molecular constraint, genetic linkage, population structure, historical contingency and so forth. Although such considerations would not change the qualitative predictions of this model, their combined effects could substantially change the predicted rate of accumulation of incompatibilities.

Finally, despite our model’s precise separation of phenotype and kryptotype, this relationship in nature may be far more complicated as aspects of the kryptotype may be less “hidden” than we currently assume. For instance, attributes excluded from the phenotype as modelled here, ignore the potential energy costs associated with excessively large (non-minimal) kryptotypes, as well as the relationship between a specific network architecture and robustness to mutational, transcriptional, or environmental noise. More precise modeling will require better mechanistic understanding not only of biological systems, but also the nature of selective pressures and genetic variation in these systems.

Acknowledgements

We would like to thank Sergey Nuzhdin, Stevan Arnold, Erik Lundgren, and Hossein Asgharian for valuable discussion.

Josh: please fix capitalization in the references. To do this, anything that needs to be capitalized gets put in curly braces, which tells bibtex to render the capitalization 'as-is'.

References

- BDO Anderson, RW Newcomb, RE Kalman, and DC Youla. Equivalence of linear time-invariant dynamical systems. *Journal of the Franklin Institute*, 281(5):371–378, 1966. 1, 5
- Stevan J. Arnold, Reinhard Brger, Paul A. Hohenlohe, Beverley C. Ajie, and Adam G. Jones. Understanding the evolution and stability of the G-matrix. *Evolution*, 62(10):2451–2461, 2008. ISSN 1558-5646. doi: 10.1111/j.1558-5646.2008.00472.x. URL <http://dx.doi.org/10.1111/j.1558-5646.2008.00472.x>. 11
- Anthony J Barley, Jordan White, Arvin C Diesmos, and Rafe M Brown. The challenge of species delimitation at the extremes: diversification without morphological change in philippine sun skinks. *Evolution*, 67(12): 3556–3572, 2013. 14
- N. H. Barton. What role does natural selection play in speciation? *Philosophical Transactions of the Royal Society of London B: Biological Sciences*, 365(1547):1825–1840, 2010. ISSN 0962-8436. doi: 10.1098/rstb.2010.0001. URL <http://rstb.royalsocietypublishing.org/content/365/1547/1825>. 2
- Nick H Barton, Alison M Etheridge, and Amandine Véber. The infinitesimal model. *bioRxiv*, 2016. doi: 10.1101/039768. URL <http://biorxiv.org/content/early/2016/02/15/039768>. 11, 23
- Richard Ernest Bellman and Karl Johan Åström. On structural identifiability. *Mathematical biosciences*, 7 (3-4):329–339, 1970. 1
- Aviv Bergman and Mark L Siegal. Evolutionary capacitance as a general feature of complex gene networks. *Nature*, 424(6948):549–552, 2003. 1
- Aleksandra A. Chertkova, Joshua S. Schiffman, Sergey V. Nuzhdin, Konstantin N. Kozlov, Maria G. Samsonova, and Vitaly V. Gursky. In silico evolution of the drosophila gap gene regulatory sequence under elevated mutational pressure. *BMC Evolutionary Biology*, 17(1):4, 2017. ISSN 1471-2148. doi: 10.1186/s12862-016-0866-y. URL <http://dx.doi.org/10.1186/s12862-016-0866-y>. 1
- Joseph D Coolon, C Joel McManus, Kraig R Stevenson, Brenton R Graveley, and Patricia J Wittkopp. Tempo and mode of regulatory evolution in drosophila. *Genome research*, 24(5):797–808, 2014. 14
- Jerry A Coyne and H Allen Orr. The evolutionary genetics of speciation. *Philosophical Transactions of the Royal Society of London B: Biological Sciences*, 353(1366):287–305, 1998. 10, 14
- Gheorghe Craciun and Casian Pantea. Identifiability of chemical reaction networks. *Journal of Mathematical Chemistry*, 44(1):244–259, 2008. 1
- Bernard Crespi and Patrik Nosil. Conflictual speciation: species formation via genomic conflict. *Trends in ecology & evolution*, 28(1):48–57, 2013. 15
- Anton Crombach, Karl R Wotton, Eva Jiménez-Guri, and Johannes Jaeger. Gap gene regulatory dynamics evolve along a genotype network. *Molecular biology and evolution*, 33(5):1293–1307, 2016. 1, 14
- Chiraj K Dalal and Alexander D Johnson. How transcription circuits explore alternative architectures while maintaining overall circuit output. *Genes & Development*, 31(14):1397–1405, 2017. 2, 14

- Chiraj K Dalal, Ignacio A Zuleta, Kaitlin F Mitchell, David R Andes, Hana El-Samad, and Alexander D Johnson. Transcriptional rewiring over evolutionary timescales changes quantitative and qualitative properties of gene expression. *Elife*, 5:e18981, 2016. [2](#)
- Eric H Davidson and Douglas H Erwin. Gene regulatory networks and the evolution of animal body plans. *Science*, 311(5762):796–800, 2006. [1](#)
- Jeremy Draghi and Michael Whitlock. Robustness to noise in gene expression evolves despite epistatic constraints in a model of gene networks. *Evolution*, 69(9):2345–2358, 2015. [1](#)
- Gerald M Edelman and Joseph A Gally. Degeneracy and complexity in biological systems. *Proceedings of the National Academy of Sciences*, 98(24):13763–13768, 2001. [1](#)
- JC Fay and PJ Wittkopp. Evaluating the role of natural selection in the evolution of gene regulation. *Heredity*, 100(2):191–199, 2008. [15](#)
- Janna L Fierst and Thomas F Hansen. Genetic architecture and postzygotic reproductive isolation: evolution of bateson-dobzhansky-muller incompatibilities in a polygenic model. *Evolution*, 2009. [2](#), [14](#)
- Jackie Gavin-Smyth and Daniel R Matute. Embryonic lethality leads to hybrid male inviability in hybrids between drosophila melanogaster and d. santomea. *Ecology and evolution*, 3(6):1580–1589, 2013. [14](#)
- M Grewal and K Glover. Identifiability of linear and nonlinear dynamical systems. *IEEE Transactions on automatic control*, 21(6):833–837, Dec 1976. doi: 10.1109/TAC.1976.1101375. [1](#)
- Ryan N Gutenkunst, Joshua J Waterfall, Fergal P Casey, Kevin S Brown, Christopher R Myers, and James P Sethna. Universally sloppy parameter sensitivities in systems biology models. *PLoS computational biology*, 3(10):e189, 2007. [15](#)
- Wilfried Haerty and Rama S Singh. Gene regulation divergence is a major contributor to the evolution of dobzhansky–muller incompatibilities between species of drosophila. *Molecular Biology and Evolution*, 23(9):1707–1714, 2006. [14](#)
- J BS Haldane. Sex ratio and unisexual sterility in hybrid animals. *Journal of genetics*, 12(2):101–109, 1922. [10](#)
- Thomas F. Hansen and Emilia P. Martins. Translating between microevolutionary process and macroevolutionary patterns: The correlation structure of interspecific data. *Evolution*, 50(4):1404–1417, 1996. ISSN 00143820, 15585646. URL <http://www.jstor.org/stable/2410878>. [22](#), [23](#)
- Emily E Hare, Brant K Peterson, Venky N Iyer, Rudolf Meier, and Michael B Eisen. Sepsid even-skipped enhancers are functionally conserved in drosophila despite lack of sequence conservation. *PLoS Genet*, 4(6):e1000106, 2008. [2](#)
- S Blair Hedges, Julie Marin, Michael Suleski, Madeline Paymer, and Sudhir Kumar. Tree of life reveals clock-like speciation and diversification. *Molecular biology and evolution*, 32(4):835–845, 2015. [15](#)
- Jennifer W Israel, Megan L Martik, Maria Byrne, Elizabeth C Raff, Rudolf A Raff, David R McClay, and Gregory A Wray. Comparative developmental transcriptomics reveals rewiring of a highly conserved gene regulatory network during a major life history switch in the sea urchin genus heliocardaris. *PLoS Biol*, 14(3):e1002391, 2016. [1](#)
- Johannes Jaeger. The gap gene network. *Cellular and Molecular Life Sciences*, 68(2):243–274, 2011. [1](#)
- Johannes Jaeger, Svetlana Surkova, Maxim Blagov, Hilde Janssens, David Kosman, Konstantin N Kozlov, Ekaterina Myasnikova, Carlos E Vanario-Alonso, Maria Samsonova, David H Sharp, et al. Dynamic control of positional information in the early drosophila embryo. *Nature*, 430(6997):368–371, 2004. [1](#)

- Johannes Jaeger, Manfred Laubichler, and Werner Callebaut. The comet cometh: evolving developmental systems. *Biological theory*, 10(1):36–49, 2015. 1
- Alexander D Johnson. The rewiring of transcription circuits in evolution. *Current Opinion in Genetics & Development*, 47:121–127, 2017. 14
- R. E. 1930-(Rudolf Emil) Kalman, Peter L. Falb, and Michael A. Arbib. *Topics in mathematical system theory*. McGraw-Hill, New York, 1969. ISBN 0754321069. 5
- Rudolf Emil Kalman. Mathematical description of linear dynamical systems. *J.S.I.A.M Control*, 1963. 1, 5, 14
- M. Kasowski, F. Grubert, C. Heffelfinger, M. Hariharan, A. Asabere, S. M. Waszak, L. Habegger, J. Rozowsky, M. Shi, A. E. Urban, M. Y. Hong, K. J. Karczewski, W. Huber, S. M. Weissman, M. B. Gerstein, J. O. Korbel, and M. Snyder. Variation in transcription factor binding among humans. *Science*, 328(5975):232–235, April 2010. 14
- Motoo Kimura. Possibility of extensive neutral evolution under stabilizing selection with special reference to nonrandom usage of synonymous codons. *Proceedings of the National Academy of Sciences*, 78(9):5773–5777, 1981. 2
- Eugene V Koonin. Splendor and misery of adaptation, or the importance of neutral null for understanding evolution. *BMC biology*, 14(1):114, 2016. 15
- Konstantin Kozlov, Svetlana Surkova, Ekaterina Myasnikova, John Reinitz, and Maria Samsonova. Modeling of gap gene expression in *Drosophila Kruppel* mutants. *PLoS Computational Biology*, 2012. 1
- Konstantin Kozlov, Vitaly Gursky, Ivan Kulakovskiy, and Maria Samsonova. Sequence-based model of gap gene regulatory network. *BMC Genomics*, 2014. 1
- Konstantin Kozlov, Vitaly V Gursky, Ivan V Kulakovskiy, Arina Dymova, and Maria Samsonova. Analysis of functional importance of binding sites in the *Drosophila* gap gene network model. *BMC Genomics*, 2015. 1
- Russell Lande. Models of speciation by sexual selection on polygenic traits. *Proceedings of the National Academy of Sciences*, 78(6):3721–3725, 1981. URL <http://www.pnas.org/content/78/6/3721.abstract>. 11, 23
- Tuuli Lappalainen, Michael Sammeth, Marc R Friedländer, Peter ACt Hoen, Jean Monlong, Manuel A Rivas, Mar Gonzalez-Porta, Natalja Kurbatova, Thasso Griebel, Pedro G Ferreira, et al. Transcriptome and genome sequencing uncovers functional variation in humans. *Nature*, 501(7468):506–511, 2013. 14
- Hugo Lavoie, Hervé Hogues, Jaideep Mallick, Adnane Sellam, André Nantel, and Malcolm Whiteway. Evolutionary tinkering with conserved components of a transcriptional regulatory network. *PLoS Biol*, 8(3):e1000329, 2010. 2
- Dorothea Lindtke and C Alex Buerkle. The genetic architecture of hybrid incompatibilities and their effect on barriers to introgression in secondary contact. *Evolution*, 69(8):1987–2004, 2015. 14
- Michael Lynch. The frailty of adaptive hypotheses for the origins of organismal complexity. *Proceedings of the National Academy of Sciences*, 104(suppl 1):8597–8604, 2007. 15
- Michael Lynch and Allan G Force. The origin of interspecific genomic incompatibility via gene duplication. *The American Naturalist*, 156(6):590–605, 2000. 14
- Katya L Mack and Michael W Nachman. Gene regulation and speciation. *Trends in Genetics*, 2016. 14

- Shamoni Maheshwari and Daniel A Barbash. Cis-by-trans regulatory divergence causes the asymmetric lethal effects of an ancestral hybrid incompatibility gene. *PLoS genetics*, 8(3):e1002597, 2012. 14
- Takeshi Matsui, Robert Linder, Joann Phan, Fabian Seidl, and Ian M Ehrenreich. Regulatory rewiring in a cross causes extensive genetic heterogeneity. *Genetics*, 201(2):769–777, 2015. 2
- Ernst Mayr. The biological species concept. *Species concepts and phylogenetic theory: a debate*. Columbia University Press, New York, pages 17–29, 2000. 7
- Pawel Michalak and Mohamed AF Noor. Association of misexpression with sterility in hybrids of *Drosophila simulans* and *D. mauritiana*. *Journal of molecular evolution*, 59(2):277–282, 2004. 14
- Eric Mjolsness, David H Sharp, and John Reinitz. A connectionist model of development. *Journal of theoretical Biology*, 152(4):429–453, 1991. 1
- Masatoshi Nei, Takeo Maruyama, and Chung-I Wu. Models of evolution of reproductive isolation. *Genetics*, 103(3):557–579, 1983. 14
- H Allen Orr. Haldane’s rule. *Annual Review of Ecology and Systematics*, 28(1):195–218, 1997. 10
- H Allen Orr, John P Masly, and Daven C Presgraves. Speciation genes. *Current opinion in genetics & development*, 14(6):675–679, 2004. 15
- Michael E Palmer and Marcus W Feldman. Dynamics of hybrid incompatibility in gene networks in a constant environment. *Evolution*, 63(2):418–431, 2009. 14
- Mihaela Pavlicev and Günter P Wagner. A model of developmental evolution: selection, pleiotropy and compensation. *Trends in Ecology & Evolution*, 27(6):316–322, 2012. 1
- Y.P. Petrov and V.S. Sizikov. *Well-posed, ill-posed, and intermediate problems with applications*, volume 49. Walter de Gruyter, 2005. 2
- Matthew Piazza, Xiao-Jiang Feng, Joshua D Rabinowitz, and Herschel Rabitz. Diverse metabolic model parameters generate similar methionine cycle dynamics. *Journal of theoretical biology*, 251(4):628–639, 2008. 15
- Björn Plötner, Markus Nurmi, Axel Fischer, Mutsumi Watanabe, Korbinian Schneeberger, Svante Holm, Neha Vaid, Mark Aurel Schöttler, Dirk Walther, Rainer Hoefgen, et al. Chlorosis caused by two recessively interacting genes reveals a role of rna helicase in hybrid breakdown in *Arabidopsis thaliana*. *The Plant Journal*, 2017. 14
- Adam H Porter and Norman A Johnson. Speciation despite gene flow when developmental pathways evolve. *Evolution*, 56(11):2103–2111, 2002. 2, 14
- Daven C Presgraves. The molecular evolutionary basis of species formation. *Nature Reviews Genetics*, 11(3):175–180, 2010. 15
- Camille Roux, Christelle Fraise, Jonathan Romiguier, Yoann Anciaux, Nicolas Galtier, and Nicolas Bierne. Shedding light on the grey zone of speciation along a continuum of genomic divergence. *PLoS biology*, 14(12):e2000234, 2016. 15
- Dolph Schluter. Evidence for ecological speciation and its alternative. *Science*, 323(5915):737–741, 2009. 15
- Ole Seehausen, Roger K Butlin, Irene Keller, Catherine E Wagner, Janette W Boughman, Paul A Hohenlohe, Catherine L Peichel, Glenn-Peter Saetre, Claudia Bank, Åke Brännström, et al. Genomics and the origin of species. *Nature Reviews Genetics*, 15(3):176–192, 2014. 14

- Maria R Servedio, Yaniv Brandvain, Sumit Dhole, Courtney L Fitzpatrick, Emma E Goldberg, Caitlin A Stern, Jeremy Van Cleve, and D Justin Yeh. Not just a theory the utility of mathematical models in evolutionary biology. *PLoS Biol*, 12(12):e1002017, 2014. 1
- Mark L Siegal and Aviv Bergman. Waddington’s canalization revisited: developmental stability and evolution. *Proceedings of the National Academy of Sciences*, 99(16):10528–10532, 2002. 1
- K. Stefflova, D. Thybert, M. D. Wilson, I. Streeter, J. Aleksic, P. Karagianni, A. Brazma, D. J. Adams, I. Talianidis, J. C. Marioni, P. Flicek, and D. T. Odom. Cooperativity and rapid evolution of cobound transcription factors in closely related mammals. *Cell*, 154(3):530–540, August 2013. 13
- Amos Tanay, Aviv Regev, and Ron Shamir. Conservation and evolvability in regulatory networks: the evolution of ribosomal regulation in yeast. *Proceedings of the National Academy of Sciences of the United States of America*, 102(20):7203–7208, 2005. 2
- John R True and Eric S Haag. Developmental system drift and flexibility in evolutionary trajectories. *Evolution & development*, 3(2):109–119, 2001. 1, 2, 14
- Annie E Tsong, Brian B Tuch, Hao Li, and Alexander D Johnson. Evolution of alternative transcriptional circuits with identical logic. *Nature*, 443(7110):415–420, 2006. 2
- Alexander Y Tulchinsky, Norman A Johnson, Ward B Watt, and Adam H Porter. Hybrid incompatibility arises in a sequence-based bioenergetic model of transcription factor binding. *Genetics*, 198(3):1155–1166, 2014. 2
- M Turelli and N H Barton. Genetic and statistical analyses of strong selection on polygenic traits: what, me normal? *Genetics*, 138(3):913–941, November 1994. URL <https://www.ncbi.nlm.nih.gov/pmc/articles/PMC1206238/>. 15
- Michael Turelli and H Allen Orr. The dominance theory of haldane’s rule. *Genetics*, 140(1):389–402, 1995. 10
- AJ Van der Schaft. Equivalence of dynamical systems by bisimulation. *IEEE transactions on automatic control*, 49(12):2160–2172, 2004. 1
- Dominique J Verlaan, Bing Ge, Elin Grundberg, Rose Hoberman, Kevin CL Lam, Vonda Koka, Joana Dias, Scott Gurd, Nicolas W Martin, Hans Mallmin, et al. Targeted screening of cis-regulatory variation in human haplotypes. *Genome research*, 19(1):118–127, 2009. 14
- Jeff Vierstra, Eric Rynes, Richard Sandstrom, Miaohua Zhang, Theresa Canfield, R Scott Hansen, Sandra Stehling-Sun, Peter J Sabo, Rachel Byron, Richard Humbert, et al. Mouse regulatory dna landscapes reveal global principles of cis-regulatory evolution. *Science*, 346(6212):1007–1012, 2014. 2
- Andreas Wagner. Evolution of gene networks by gene duplications: a mathematical model and its implications on genome organization. *Proceedings of the National Academy of Sciences*, 91(10):4387–4391, 1994. 1
- Andreas Wagner. Does evolutionary plasticity evolve? *Evolution*, pages 1008–1023, 1996. 1
- Eric Walter, Yves Lecourtier, and John Happel. On the structural output distinguishability of parametric models, and its relations with structural identifiability. *IEEE Transactions on Automatic Control*, 29(1): 56–57, 1984. 1
- Kenneth M Weiss and Stephanie M Fullerton. Phenogenetic drift and the evolution of genotype–phenotype relationships. *Theoretical population biology*, 57(3):187–195, 2000. 1, 14

Karl R Wotton, Eva Jiménez-Guri, Anton Crombach, Hilde Janssens, Anna Alcaine-Colet, Steffen Lemke, Urs Schmidt-Ott, and Johannes Jaeger. Quantitative system drift compensates for altered maternal inputs to the gap gene network of the scuttle fly *megascelia abdita*. *Elife*, 4:e04785, 2015. [1](#), [14](#)

Lotfi A Zadeh and Charles A Deoser. *Linear system theory*. Robert E. Krieger Publishing Company Huntington, 1976. [1](#)

A Local expansion of the fitness surface

A.1 Away from the optimum

Let two points on \mathcal{N} be x_1 and x_2 , let $\bar{x} = (x_1 + x_2)/2$, and let $z = (x_2 - x_1)/2$. Then with ∇D and $\nabla^2 D$ the first and second derivatives of D , respectively, Taylor expanding about x_1 and x_2 finds that

$$\begin{aligned} D(\bar{x}) &= D(x_1) + \nabla D(x_1) \cdot z + \frac{1}{2} z^T \nabla^2 D(x_1) z + O(\|z\|^3) \\ &= D(x_2) - \nabla D(x_2) \cdot z + \frac{1}{2} z^T \nabla^2 D(x_2) z + O(\|z\|^3). \end{aligned}$$

Now, since $D(x_1) = D(x_2) = \nabla D(x_1) = \nabla D(x_2) = 0$ and

$$\begin{aligned} \nabla D(x_2) &= \nabla D(x_1) + 2z^T \nabla^2 D(x_1) + O(\|z\|^2), \quad \text{and} \\ \nabla^2 D(x_2) &= \nabla^2 D(x_1) + O(\|z\|), \end{aligned}$$

adding together the two equations above and dividing by two gets that

$$D(\bar{x}) = \Phi_0 - \frac{3}{2} z^T \nabla^2 D(x_1) z + O(\|z\|^3).$$

A.2 Differentiating the fitness function

Suppose that $\rho(t) \geq 0$ is a weighting function on $[0, \infty)$ so that fitness is a function of $L^2(\rho)$ distance of the impulse response from optimal. With $h_0(t) = C_0 e^{tA_0} B_0$ a representative of the optimal set:

$$\begin{aligned} D(A, B, C)^2 &:= \int_0^\infty \rho(t) |h_A(t) - h_0(t)|^2 dt \\ &:= \int_0^\infty \rho(t) |C e^{At} B - C_0 e^{A_0 t} B_0|^2 dt \\ &= \int_0^\infty \rho(t) \operatorname{tr} \left\{ (C e^{At} B - C_0 e^{A_0 t} B_0)^T (C e^{At} B - C_0 e^{A_0 t} B_0) \right\} dt \\ &= \int_0^\infty \rho(t) \operatorname{tr} \left\{ (C e^{At} B - C_0 e^{A_0 t} B_0) (C e^{At} B - C_0 e^{A_0 t} B_0)^T \right\} dt, \end{aligned} \tag{8}$$

where $\operatorname{tr} X$ denotes the trace of a square matrix X . How does this change as we perturb about (A_0, B_0, C_0) ? First we differentiate with respect to A , keeping $B = B_0$ and $C = C_0$ fixed. Since

$$\frac{d}{du} e^{(A+uZ)t} \Big|_{u=0} = \int_0^t e^{As} Z e^{A(t-s)} ds, \tag{9}$$

we have that

$$\begin{aligned} \frac{d}{du} D(A + uZ, B_0, C_0)^2 \Big|_{u=0} &= 2 \int_0^\infty \rho(t) \operatorname{tr} \left\{ C_0 \left(\int_0^t e^{As} Z e^{A(t-s)} ds \right) B_0 B_0^T (e^{At} - e^{A_0 t})^T C_0^T \right\} dt \\ &= 2 \int_0^\infty \rho(t) \operatorname{tr} \left\{ C_0 \left(\int_0^t e^{As} Z e^{A(t-s)} ds \right) B_0 (h_A(t) - h_0(t))^T \right\} dt \end{aligned} \tag{10}$$

and, by differentiating this and supposing that A is on the optimal set, i.e., $h_A(t) = h_0(t)$, (so without loss of generality, $A = A_0$):

$$\begin{aligned}\mathcal{H}^{A,A}(Y, Z) &:= \frac{1}{2} \frac{d}{du} \frac{d}{dv} D(A_0 + uY + vZ, B_0, C_0)^2|_{u=v=0} \\ &= \int_0^\infty \rho(t) \operatorname{tr} \left\{ C_0 \left(\int_0^t e^{A_0 s} Y e^{A_0(t-s)} ds \right) B_0 B_0^T \left(\int_0^t e^{A_0 s} Z e^{A_0(t-s)} ds \right)^T C_0^T \right\} dt.\end{aligned}\quad (11)$$

The function \mathcal{H} will define a quadratic form. To illustrate the use of this, suppose that B and C are fixed. By defining Δ_{ij} to be the matrix with a 1 in the (i, j) th slot and 0 elsewhere, the coefficients of the quadratic form is

$$H_{ij, k\ell}(A) := \mathcal{H}(\Delta_{ij}, \Delta_{k\ell}). \quad (12)$$

We could use this to get the quadratic approximation to D near the optimal set. To do so, it'd be nice to have a way to compute the inner integral above. Suppose that we diagonalize $A = U\Lambda U^{-1}$. Then

$$\int_0^t e^{As} Z e^{A(t-s)} ds = \int_0^t U e^{\Lambda s} U^{-1} Z U e^{\Lambda(t-s)} U^{-1} ds \quad (13)$$

Now, notice that

$$\int_0^t e^{s\lambda_i} e^{(t-s)\lambda_j} ds = \frac{e^{t\lambda_i} - e^{t\lambda_j}}{\lambda_i - \lambda_j}. \quad (14)$$

Therefore, defining

$$X_{ij}(t, Z) = (U^{-1} Z U)_{ij} \frac{e^{t\lambda_i} - e^{t\lambda_j}}{\lambda_i - \lambda_j} \quad (15)$$

moving the U and U^{-1} outside the integral and integrating we get that

$$\int_0^t e^{As} Z e^{A(t-s)} ds = U X(t, Z) U^{-1}. \quad (16)$$

Following on from above, we see that if $Z = \Delta_{k\ell}$, then

$$X_{ij}^{k\ell}(t) = \frac{e^{t\lambda_i} - e^{t\lambda_j}}{\lambda_i - \lambda_j} (U^{-1})_{\cdot k} U_{\ell \cdot}, \quad (17)$$

where $U_{k\cdot}$ is the k th row of U , and so

$$H_{ij, k\ell}(A) = \int_0^\infty \rho(t) \operatorname{tr} \{ C U X^{ij}(t) U^{-1} B B^T (U^{-1})^T X^{k\ell}(t)^T U^T C^T \} dt. \quad (18)$$

This implies that

$$D(A_0 + \epsilon Z)^2 \approx \epsilon^2 \sum_{ij, k\ell} H^{ij, k\ell} Z_{ij} Z_{k\ell} \quad (19)$$

and so

$$D(A_0 + \epsilon Z)^2 \approx \epsilon^2 \sum_{ij, k\ell} H^{ij, k\ell} Z_{ij} Z_{k\ell} \quad (20)$$

By section [B](#), if we set $\Sigma = \sigma^2 I$ and $U = H$, then a population at $A_0 + Z$ experiences a restoring force of strength $(I + \sigma^2 H^{-1})^{-1} Z$ (treating Z as a vector and H as an operator on these). If σ^2 is small compared to H^{-1} then this is approximately $-\sigma^2 H^{-1} Z$. This suggests that the population mean follows an Ornstein-Uhlenbeck process, as described (in different terms) in [Hansen and Martins \[1996\]](#).

More generally, B and C may also change. To extend this we need the remaining second derivatives of D^2 . First, in B :

$$\begin{aligned}\mathcal{H}^{B,B}(Y, Z) &:= \frac{1}{2} \frac{d}{du} \frac{d}{dv} D(A_0, B_0 + uY + vZ, C_0)|_{u=v=0} \\ &= \frac{1}{2} \int_0^\infty \rho(t) \operatorname{tr} \left\{ C_0 e^{tA_0} \frac{d}{du} \frac{d}{dv} (uY + vZ)(uY + vZ)^T |_{u=v=0} e^{tA_0^T} C_0^T \right\} dt \\ &= \frac{1}{2} \int_0^\infty \rho(t) \operatorname{tr} \left\{ C_0 e^{tA_0} (YZ^T + ZY^T) e^{tA_0^T} C_0^T \right\} dt.\end{aligned}\tag{21}$$

Next, in C :

$$\begin{aligned}\mathcal{H}^{B,B}(Y, Z) &:= \frac{1}{2} \frac{d}{du} \frac{d}{dv} D(A_0, B_0, C_0 + uY + vZ)|_{u=v=0} \\ &= \frac{1}{2} \int_0^\infty \rho(t) \operatorname{tr} \left\{ B_0 e^{tA_0^T} \frac{d}{du} \frac{d}{dv} (uY + vZ)^T (uY + vZ) |_{u=v=0} e^{tA_0} B_0 \right\} dt \\ &= \frac{1}{2} \int_0^\infty \rho(t) \operatorname{tr} \left\{ B_0 e^{tA_0^T} (YZ^T + ZY^T) e^{tA_0} B_0 \right\} dt.\end{aligned}\tag{22}$$

Now, the mixed derivatives in B and C :

$$\begin{aligned}\mathcal{H}^{B,C}(Y, Z) &:= \frac{1}{2} \frac{d}{du} \frac{d}{dv} D(A_0, B_0 + uY, C_0 + vZ)|_{u=v=0} \\ &= \int_0^\infty \rho(t) \operatorname{tr} \left\{ Y e^{tA_0^T} C_0^T Z e^{tA_0} B_0 \right\} dt.\end{aligned}\tag{23}$$

In A and B

$$\begin{aligned}\mathcal{H}^{A,B}(Y, Z) &:= \frac{1}{2} \frac{d}{du} \frac{d}{dv} D(A_0 + uY, B_0 + vZ, C_0)|_{u=v=0} \\ &= \int_0^\infty \rho(t) \operatorname{tr} \left\{ C_0 \left(\int_0^t e^{sA_0} Y e^{(t-s)A_0} ds \right) B_0 Z^T e^{tA_0} C_0 \right\} dt,\end{aligned}\tag{24}$$

and finally in A and C :

$$\begin{aligned}\mathcal{H}^{A,C}(Y, Z) &:= \frac{1}{2} \frac{d}{du} \frac{d}{dv} D(A_0 + uY, B_0, C_0 + vZ)|_{u=v=0} \\ &= \int_0^\infty \rho(t) \operatorname{tr} \left\{ C_0 \left(\int_0^t e^{sA_0} Y e^{(t-s)A_0} ds \right) B_0 B_0 e^{tA_0} Z \right\} dt.\end{aligned}\tag{25}$$

Together, numerical computation of these expressions, along with estimates of genetic covariance within a population, allow precise predictions of evolutionary dynamics of a particular system. The approximation should be good as long as the second-order Taylor approximation holds.

B Genetic drift with a multivariate trait

For completeness, we provide a brief exposition of how a population evolves due to genetic drift with a quantitative genetics model, as in [Lande \[1981\]](#) or [Hansen and Martins \[1996\]](#). These do not directly model underlying genetic basis, but developing a more accurate model is beyond the scope of this paper.

Suppose that the population is distributed in trait space as a Gaussian with covariance matrix Σ and mean μ , whose density we write as $f(\cdot; \Sigma, \mu)$. Selection has the effect of multiplying this density by the fitness function and renormalizing, so that if expected fitness of x is proportional to $\exp(-\|Lx\|^2/2)$, then the distribution post-selection has density at x proportional to $f(x; \Sigma, \mu) \exp(-\|Lx\|^2/2)$. By the computation below (“Completing the square”), the result is a Gaussian distribution with covariance matrix $(\Sigma^{-1} + L^T L)^{-1}$ and mean $(\Sigma^{-1} + L^T L)^{-1} \Sigma^{-1} \mu$.

After selection, we have reproduction: suppose this occurs as in the infinitesimal model [Barton et al., 2016], so that each offspring of parents with traits x and y is drawn independently from a Gaussian distribution with mean $(x + y)/2$ and covariance matrix R . Here, R is the contribution of “segregation variance”, i.e., random choices of parental alleles. If $\tilde{\Sigma} = (\Sigma^{-1} + L^T L)^{-1}$ is the covariance matrix of the parents post-selection, then the distribution of offspring will again be Gaussian, with mean equal to that of the parents and covariance matrix $\tilde{\Sigma}/2 + R$.

In summary, a generation under this model modifies the mean (μ) and covariance matrix (Σ) of a population as follows:

$$\begin{aligned}\mu &\mapsto \mu' = (\Sigma^{-1} + L^T L)^{-1} \Sigma^{-1} \mu \\ \Sigma &\mapsto \Sigma' = \frac{1}{2}(\Sigma^{-1} + L^T L)^{-1} + R.\end{aligned}$$

What measures are stable under this transformation? The condition $\mu = \mu'$ reduces to $\Sigma L^T L \mu = 0$; if we assume R and therefore Σ are of full rank, then this happens if and only if μ is in the null space of L , i.e., if μ lies in a neutral direction. The condition $\Sigma' = \Sigma$ can also be solved, at least numerically. After rearrangement, it reduces to $\Sigma L^T L \Sigma + (I/2 - R L^T L) \Sigma = R$. Importantly, the mean μ does not affect either how the covariance matrix moves, or its stable shape.

Above we have described the *expected* motion of the mean and covariance. However, random resampling will introduce noise. Suppose that a population of N individuals behaves approximately as described above. By the above, we may expect that the covariance matrix stays close to a constant value Σ , computed from R and L as above, so that we need only consider motion of the mean, μ . Since we take a sample of size N to construct the next generation, the next generation’s mean is drawn from a Gaussian distribution with mean μ' and covariance matrix Σ/N . Defining $\Gamma = (I - (I + \Sigma L^T L)^{-1})$, this can be written as

$$\mu' - \mu = \Gamma \mu + \epsilon / \sqrt{N},$$

where ϵ is a multivariate Gaussian with mean zero and covariance matrix Σ . Let $\mu(k)$ denote the mean in the k^{th} generation, and suppose that μ differs from optimal by something of order $1/\sqrt{N}$: if $\nu(t) = \sqrt{N} \mu(t\sqrt{N})$ is the rescaled process, then the previous equation implies that as $N \rightarrow \infty$, in the limit ν solves the Itô equation

$$d\nu(t) = \Gamma \nu(t) dt + \Sigma^{1/2} dW(t),$$

where now $W(t)$ is a multivariate white noise. This has an explicit solution as a multivariate Ornstein-Uhlenbeck process:

$$\nu(t) = e^{-t\Gamma} \nu(0) + \int_0^t e^{-(t-s)\Gamma} \Sigma^{1/2} dW(s).$$

The asymptotic variance of this process in the direction z is

$$\lim_{t \rightarrow \infty} \text{Var}[\nu(t) \cdot z] = \int_0^\infty z^T e^{-s\Gamma} \Sigma e^{-s\Gamma} z ds, \quad (26)$$

which is infinite if and only if $\Gamma z = 0$, which occurs if and only if $Lz = 0$. This implies that at equilibrium, population mean trait values lie away from the optimal set by a Gaussian displacement of order $1/\sqrt{N}$ with a covariance matrix given by equation (26).

Completing the square First note that if A is symmetric,

$$(x - y)^T A (x - y) = x^T A (x - 2y) + y^T A y,$$

and so if B is also symmetric and $A + B$ is invertible,

$$\begin{aligned} (x - y)^T A(x - y) + x^T Bx &= x^T (A + B) (x - 2(A + B)^{-1} Ay) + y^T Ay \\ &= (x - (A + B)^{-1} Ay)^T (A + B) (x - (A + B)^{-1} Ay) \\ &\quad + y^T Ay - y^T A^T (A + B)^{-1} Ay. \end{aligned}$$

Therefore, by substituting $A = \Sigma^{-1}$ and $B = L^T L$,

$$\frac{f(x; \Sigma, y) \exp(-x^T L^T L x / 2)}{\int f(z; \Sigma, y) \exp(-z^T L^T L z / 2) dz} = f(x; (\Sigma^{-1} + L^T L)^{-1}, (\Sigma^{-1} + L^T L)^{-1} \Sigma^{-1} y).$$

B.1 Gaussian load

Suppose that a population has a Gaussian distribution in d -dimensional trait space with mean μ and covariance matrix Σ , and that fitness of an individual at x is $\exp(-\|Lx\|^2/2)$. Then, completing the square as above with $A = \Sigma^{-1}$, $y = \mu$, and $B = L^T L$, and defining $Q = (\Sigma^{-1} + L^T L)^{-1}$,

$$\begin{aligned} &\frac{1}{\sqrt{2\pi}^n \det(\Sigma)^{1/2}} \int e^{-\frac{1}{2} x^T \Sigma^{-1} x} e^{-\frac{1}{2} x^T L^T L x} dx \\ &= \frac{1}{\sqrt{2\pi}^n \det(\Sigma)^{1/2}} \int e^{-\frac{1}{2} (x - Q \Sigma^{-1} \mu)^T Q^{-1} (x - Q \Sigma^{-1} \mu)} dx \\ &\quad \times e^{\mu^T (I - \Sigma^{-1} Q) \Sigma^{-1} \mu} \\ &= \sqrt{\frac{\det(Q)}{\det(\Sigma)}} \exp\{\mu^T (I - \Sigma^{-1} Q) \Sigma^{-1} \mu\} \\ &= \sqrt{\frac{1}{\det(\Sigma) \det(\Sigma^{-1} + L^T L)}} \exp\{\mu^T (I - (I + L^T L \Sigma)^{-1}) \Sigma^{-1} \mu\} \end{aligned}$$

Now suppose that $\Sigma = \sigma^2 I$ and $L = I/\gamma$. Then,

$$\begin{aligned} \sqrt{\frac{1}{\det(\Sigma) \det(\Sigma^{-1} + L^T L)}} &= \sqrt{\frac{1}{\sigma^{2d} (1/\sigma^2 + 1/\gamma^2)^d}} \\ &= \frac{1}{(1 + (\sigma/\gamma)^2)^{d/2}}. \end{aligned}$$

Also,

$$\begin{aligned} (I - (I + L^T L \Sigma)^{-1}) \Sigma^{-1} &= \frac{1}{\sigma^2} (1 - (1 + (\sigma/\gamma)^2)^{-1}) I \\ &= \frac{1}{\gamma^2} \frac{1}{(1 + (\sigma/\gamma)^2)} I \end{aligned}$$

C Evolution of segregation covariance

The description above does not describe how *two* diverging populations interact, since the amount of *segregation variance*, quantified by R , will not stay constant. To get an idea of how this might change, suppose that a trait is determined by L unlinked, biallelic loci, and that the i^{th} locus has two alleles with additive

effects $\pm x_i$, so that being homozygous for the + allele contributes $+2x_i$ to the trait. For simplicity, we will neglect the effects of selection. If the + allele at locus i is at frequency p_i in a population, then the mean and genetic variance of the trait in a diploid population with random mating is

$$m = 2 \sum_i (2p_i - 1)x_i$$

$$s^2 = 4 \sum_i p_i(1 - p_i)x_i^2.$$

Segregation variance between two parents depends on the loci at which either are heterozygous, and each locus contributes independently since alleles are additive. If the alleles are at Hardy-Weinberg proportions, then since segregation acts like a fair coin flip, a heterozygous locus contributes $x_i^2/4$ to the variance, and so the *mean* segregation variance, averaging across parents, is

$$R_0(p) = \sum_i p_i(1 - p_i)x_i^2.$$

On the other hand, if the second parent came from a distinct population with frequencies q_i (an F_1 hybrid), this would be

$$R_1(p, q) = \frac{1}{2} \sum_i p_i^2(1 - p_i)^2 x_i^2 + \frac{1}{2} \sum_i q_i^2(1 - q_i)^2 x_i^2$$

$$= (R_0(p) + R_0(q))/2.$$

If we assume that the populations are at equilibrium, $R_0(p) \approx R_0(q)$, and so $R_1(p, q) \approx R_0(p)$.

Now consider an F_2 hybrid, where both parents are F_1 and so each heterozygous at locus i with probability $p_i(1 - q_i) + (1 - p_i)q_i$. Then

$$R_2(p, q) = \frac{1}{2} \sum_i (p_i(1 - q_i) + (1 - p_i)q_i) x_i^2.$$

Suppose that the two populations are slightly drifted from each other, with frequency difference $p_i - q_i = 2\epsilon_i$. Then,

$$p(1 - q) + p(1 - q) = (u + \epsilon)(1 - u + \epsilon) + (u - \epsilon)(1 - u - \epsilon)$$

$$= 2u(1 - u) + 2\epsilon^2.$$

If the frequencies have evolved neutrally in unconnected, Wright-Fisher populations of effective size N for t generations from a common ancestor with allele frequency u , then ϵ has mean zero and variance roughly $2u(1 - u)t/N$. Still assuming the populations are at stationarity, so that R_0 is constant between the two, and taking the frequencies p_i as a proxy for the ancestral frequencies u_i , this implies that we expect

$$R_2 \approx R_0 + 2 \sum_i p_i(1 - p_i)x_i^2 t/N$$

$$= \left(1 + \frac{2t}{N}\right) R_0.$$

On the other hand, the expected squared difference in trait *means* between two such populations is

$$8 \sum_i p_i(1 - p_i)x_i^2 t/N = 8R_0 t/N. \quad (27)$$

This implies that under this model, segregation variance in F_2 s between two populations is roughly increased by a factor of $1/8$ of the difference between their means.